Langmuir

Article

pubs.acs.org/Langmuir

Amplitude-Modulated Atomic Force Microscopy Reveals the Near Surface Nanostructure of Surfactant Sponge (L_3) and Lamellar (L_α) Phases

Marc J. Wydro,[†] Gregory G. Warr,[‡] and Rob Atkin*[,†]

[†]University of Newcastle, Newcastle, New South Wales 2308, Australia

[‡]University of Sydney, Sydney, New South Wales 2006, Australia

Supporting Information

ABSTRACT: Amplitude-modulated atomic force microscopy (AM-AFM) has been used to study the nanostructure of cetylpyridinium chloride (CPCl)−hexanol−0.2 M NaCl sponge (L_3) and lamellar (L_α) phases near a mica surface. For both phases, membrane volume fractions of 22, 27, and 32 vol % were investigated, with the L_3 or L_α phase selected by adjusting the co-surfactant/surfactant ratio (hexanol/CPCl). For the L_3 phase, the presence of the surface flattens the three-dimensional bulk structure. AM-AFM clearly resolves the membrane and solvent passages in the near surface layer. Increasing the membrane volume fraction decreases the size of the image features because of the lower solvent content. Within error, the average passage sizes in the near surface layer are the same as those in the bulk at the same concentration. Images of the L_α phase reveal undulating near surface sheets. At the highest membrane concentration, the image is very smooth, because the lamellar sheet is confined between the surface and the next near surface layer, which is in close proximity as a result of the low solvent content. As the membrane concentration is reduced, the space between layers is increased and undulations appear in the near surface lamellar structure. Undulations are more pronounced at the lowest membrane volume fraction.

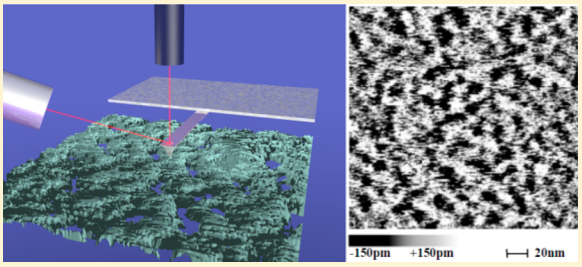

INTRODUCTION

Surfactants self-assemble into a rich variety of aggregates or liquid crystal phases depending upon their concentration and solution conditions.[1−6] When the surfactant packing geometry favors low curvature, locally bilayered structures result. On longer length scales, these bilayers arrange into various mesostructures,[2] including the sponge (L_3) and lamellar (L_α) phases.[7−9] The L_3 phase is an optically isotropic, free-flowing, bicontinuous structure comprised of randomly connected bilayers with interpercolating passages.[7,10,11] In contrast, the L_α phase is composed of undulating bilayers stacked in a one-dimensional (1D) array separated by solvent and is anisotropic and viscous.[2,12] Consistent with their structural similarities, the L_3 and L_α phases neighbor one another in the phase diagrams for numerous surfactant systems.[13−15] In some cases, it is possible to move between the L_3 and L_α phases reversibly by changing the temperature[16,17] or transforming the L_3 phase into the L_α phase by applying sufficient shear.[18−21]

The microstructure of the L_3 and L_α phases has been probed by X-ray and neutron small-angle scattering (SAS)[8,22−24] and freeze fracture electron microscopy (FFEM).[8,25,26] L_3 FFEM images revealed saddle microstructures with a clear distinction between aqueous solvent and membrane structure,[8,25,26] whereas the L_α consists of undulating stacks of bilayers as well as multi-lamellar liposomes and perforated vesicles.[8,25,26] The position of the SAS primary peak reveals the average passage diameter (d_3) of the L_3 phase and repeat spacing (d_α) for the L_α phase. In both phases, these characteristic distances scale inversely to the membrane volume fraction (ϕ) according to swelling laws.[8,24] For the cetylpyridinium chloride (CPCl)−hexanol−brine system,[15,27] the L_3 phase exists over a narrow range of hexanol/CPCl ratios but over a large range of membrane volume fractions with passage sizes ranging from nanometers to a few micrometers. Reducing the hexanol concentration moves the system though a narrow two-phase region (L_3 and L_α phases) into the large L_α phase, which is similarly stable over a wide range of membrane volume fractions.

In comparison to the L_α phase, which can stack adjacent to a solid surface, the percolating morphology of the bulk L_3 phase cannot be accommodated at an interface[15,28,29] or confined between surfaces.[17,30−32] The behavior of L_3 phases confined between surfaces was first investigated using the surface force apparatus (SFA). At large separations, L_3 phase SFA force profiles consisted of oscillations with periods equal to approximately twice the bulk d_3 distance.[17,30−32] At small separations, membrane undulations are impeded by the surfaces,[32,33] which raise the local free energy. The confined

Received: March 19, 2015
Revised: April 23, 2015
Published: April 23, 2015

DOI: 10.1021/acs.langmuir.5b01008
Langmuir 2015, 31, 5513−5520

L_3 phase undergoes a first-order phase transition to a L_α phase, with a commensurate reduction in the oscillation period.[17,30−32] Confined L_α phases also exhibit oscillating force profiles, but because there is no phase change, the oscillation period is the same for all separations.

To our knowledge, few papers have examined the structure of the L_3 phase near an isolated solid surface.[15,28,29] Neutron reflectivity studies of the CPCl−hexanol−brine system revealed that the bulk L_3 phase persisted near a quartz surface within the resolution of the measurement for low membrane volume fractions. However, at high concentrations, the L_3 to L_α phase transition was revealed, consistent with the SFA results but for an isolated interface. For intermediate concentrations, characteristic distances between those of the bulk L_3 and L_α phases were determined. This was conceptualized in two ways: as a sponge structure, which becomes increasingly distorted or spatially constrained near the surface, or as a lamellar structure, which becomes increasingly defective with distance from the surface as the number of interlayer passages increases. In this paper, we probe how the near surface nanostructure evolves laterally in the plane of the interface at these intermediate concentrations using amplitude-modulated atomic force microscopy (AM-AFM) imaging. The images obtained are contrasted with those for the L_α phase at corresponding membrane volume fractions (but different hexanol/CPCl mass ratios). We have previously used AM-AFM to image the near nanostructure of ionic liquids in contact with a solid substrate[34−37] and near surface layers and used the structures identified to rationalize ionic liquid interfacial systems,[38−40] including modeling,[35] nanotribology,[41−46] and electrical double-layer structure;[47−49] however, this is the first time that *in situ* AM-AFM has been used to study the near surface nanostructure of a surfactant mesophase. These delicate structures cannot be imaged using standard, less sensitive, AFM imaging modes. AM-AFM images are complimented by contact mode (C-AFM) force curves, which confirm the evolution of the structure with distance normal to the interface in line with that determined using neutron reflectivity.[15]

MATERIALS AND METHODS

CPCl (AJAX Finechem Pty. Ltd., 98%), hexanol (Chem-Supply Pty. Ltd., 98%), and sodium chloride (BHD Chemicals Australia Pty. Ltd., 99.9%) were used as received. Milli-Q water was used to produce the aqueous surfactant solutions. Three membrane volume fractions, 22, 27, and 32 vol %, of the L_3 and L_α phases were prepared by adjusting the co-surfactant/surfactant ratio (hexanol/CPCl).[15] L_3 phase samples were prepared with a mass ratio of 1.075 hexanol/1 CPCl, and L_α phase samples were prepared with a mass ratio of 0.9 hexanol/1 CPCl. Individual components were weighed directly into a glass vial, sealed with a Teflon-lined cap, and secured with Parafilm. Sealed vials were gently stirred at 22 °C and allowed to equilibrate overnight to produce single-phase solutions. Quantities used in the sample preparation are shown in Table 1. Samples were examined with a cross-polarized optical microscope (Carl Zeiss Optical Microscope Axioskop 40) prior to conducting AFM experiments. L_3 phase samples were optically isotropic, while L_α phase samples were birefringent with Maltese crosses.[50]

The near surface nanostructures of L_3 and L_α phases were investigated using an AFM (Bruker NanoScope 5 Multimode 8 AFM with an E vertical scanner) on a mica substrate (Brown Co., Sydney, Australia). Experiments were conducted in a temperature-controlled incubator at 22 °C. The mica substrate was prepared by cleaving along the basal plane using adhesive tape, rendering a fresh layer of atomically smooth mica. Samples were contained in a dedicated fluid cell sealed with a silicon O-ring. Immediately prior to use, both fluid cell and O-ring were rinsed with ethanol and Milli-Q water and dried with filtered nitrogen gas. The cantilever was washed with ethanol and Milli-Q water and irradiated with ultraviolet light for 15 min to ensure that all residual organic contaminants were removed.

Table 1. Composition of the Prepared L_3 and L_α Phase Samples as Weight Percentage (wt %), Volume Percentage (vol %), and Molar Fraction (mol)

phase	ϕ (vol %)	component	wt %	vol %	mol
L_3	22	CPCl	9.66	9.62	8.09×10^{-4}
		hexanol	10.35	12.34	3.04×10^{-3}
		0.2 M NaCl brine	79.99	78.04	0.9962
L_3	27	CPCl	12.04	11.91	1.01×10^{-3}
		hexanol	12.89	15.29	3.78×10^{-3}
		0.2 M NaCl brine	75.07	72.80	0.9952
L_3	32	CPCl	14.38	14.14	1.20×10^{-3}
		hexanol	15.50	18.26	4.55×10^{-3}
		0.2 M NaCl brine	70.12	67.59	0.9942
L_α	22	CPCl	10.51	10.48	8.81×10^{-4}
		hexanol	9.40	11.23	2.76×10^{-3}
		0.2 M NaCl brine	80.09	78.29	0.9964
L_α	27	CPCl	13.15	13.04	1.10×10^{-3}
		hexanol	11.88	14.11	3.49×10^{-3}
		0.2 M NaCl brine	74.97	72.85	0.9954
L_α	32	CPCl	15.65	15.43	1.31×10^{-3}
		hexanol	14.26	16.85	4.19×10^{-3}
		0.2 M NaCl brine	70.08	67.72	0.9945

Force curve data were obtained using C-AFM, whereby the cantilever deflection was monitored in response to the approach and retraction of the sample from beneath the tip.[51] A sharp silicon nitride (Si_3N_4) lever probe cantilever, SNL-10D (Bruker), was used for the L_3 phase samples, and a Si_3N_4 Scanasyst fluid probe (Bruker) was used for L_α phase samples. The spring constant for each tip was measured via the thermal noise method prior to use.[52] Nominal spring constants of SNL-10D and Scanasyst fluid probe cantilevers corresponded to k_c = 0.056 and 0.713 N m^{-1}, respectively. The scan size and scan rate for all force data were maintained between 150−250 nm and 0.2−0.5 Hz, respectively.

Height images were obtained with AM-AFM. The cantilever was oscillated at or near the resonant frequency, resulting in intermitted contact with the sample. The amplitude set point (A) was adjusted with respect to the cantilever free amplitude (A_0) such that the set point ratio (A/A_0) defines the tapping strength. Height images are established by corrections in the feedback loop in response to the piezoelectric scanner z axis as a result of changes in the cantilever oscillation.[34] A range of cantilevers were employed for imaging to compensate for viscosity changes as the phase and membrane volume fraction were changed: soft (SNL-10C, Brunker, k_c = 0.2755 N m^{-1}), intermediate (RFESP MMP-21100-10, Brunker, k_c = 1.3985 N m^{-1}; ArrowUHFAuD, Asylum Research, k_c = 5.4451 N m^{-1}), and stiff (RTESP MMP-11100-10, Brunker, k_c = 41.4520 N m^{-1}) cantilevers were used. Nominal tip radii for all cantilevers are presented in Table A of the Supporting Information. Typical scan sizes and rates ranged from 100 to 400 nm and from 1.25 to 2.25 Hz, respectively.

RESULTS AND DISCUSSION

C-AFM force data for the CPCl−hexanol−0.2 M NaCl L_3 phase with mass ratio (1.075 hexanol/1 CPCl) are presented in Figure 1 for membrane (CPCl + hexanol) volume fractions of 22, 27, and 32 vol %. The appearance of the force data is qualitatively similar to that reported previously using SFA for similar L_3 phase systems,[17,30−32] except that the long-range attraction noted with SFA is absent. In the SFA data, the long-range attraction was attributed to a capillary force, resulting from condensation of a L_α phase between the approaching

DOI: 10.1021/acs.langmuir.5b01008
Langmuir 2015, 31, 5513−5520

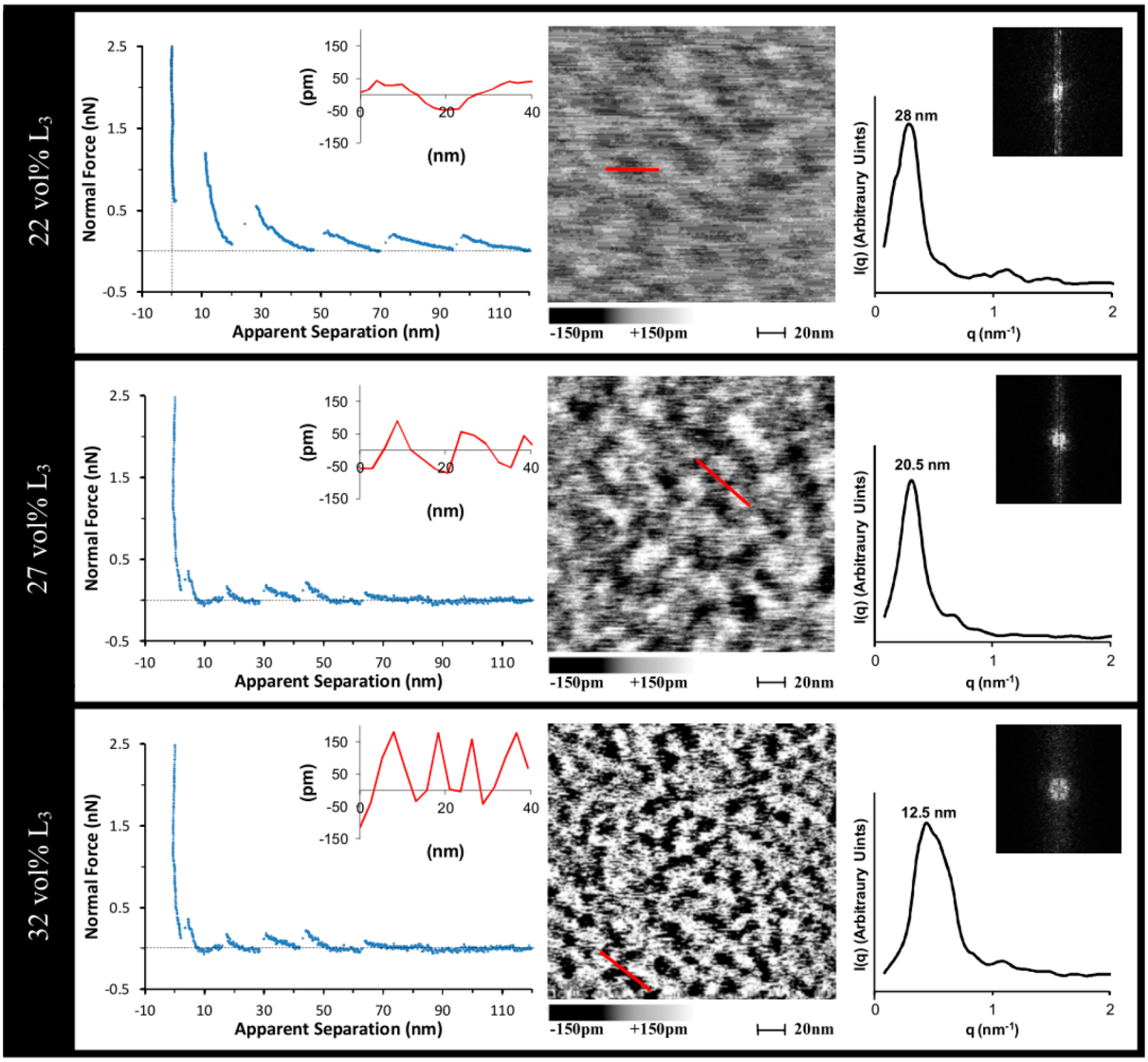

Figure 1. Near surface interfacial data for the L_3 system over a range of membrane volume fractions (ϕ = 22, 27, and 32 vol %). Column 1 shows typical force profiles as recorded by the approach of the substrate and AFM tip, with the x axis measuring the displacement of the AFM piezo scanners and the y axis monitoring the force corresponding to deflection of the tip. The inset shows the vertical height variation over a small transect from a cross-sectional cut in column 2. Column 2 shows height images, with dark areas corresponding to areas of depression relating to passages and the red line corresponding to the cross-sectional cut related to the inset in column 1. Column 3 shows the 2D FTs (inset) and the associated radially averaged 1D plot displaying the q value related to the mean periodic spacing.

surfaces. The absence of a long-range attraction here may be a consequence of the tip and surface being different materials[53] or the small size of the AFM tip hindering capillary condensation.

As the AFM tip moves toward the surface, a series of oscillations (compressions and ruptures) are measured from ~120 nm. For each oscillation, the compression first leads to the solvent being displaced from between membranes, while the membrane thickness remains constant.[31] As the separation is further decreased, the repulsion increases as oscillations of bilayers between the tip and the surface are impeded, which eventually leads to the creation of an edge dislocation. Once a critical force is reached, a dislocation loop nucleates, leading to membrane expulsion and a rapid reduction in force. Because the contribution of edge dislocation to free energy is small, the change in force with separation is elastic and the data have the form of a series of parabolas,[17,31,32] which can be fit using a previously reported model.[54,55] Fitting allows the compressibility modulus ($\overline{B}$) and oscillation period to be extracted. These fits are shown in Figure A of the Supporting Information.

The fitted oscillation periods are between 1 and 2 times the bulk phase passage diameters (characteristic distance) and are consistent with earlier reports.[17,31,32] Because the AFM tip radii were not measured, the fitted $\overline{B}$ data cannot be treated quantitatively. However, because the same tip was used for all of the L_3 phase force data, qualitative comparisons can be made. The $\overline{B}$ values and the oscillation period both decrease (see Figure A of the Supporting Information) with increasing the membrane volume fraction. This is because as the membrane volume fraction increases, the solvent volume decreases, meaning membranes are packed together more tightly and, thus, interact more strongly. At each concentration, the model fits the data well at large separations but fails at short distances; closer to the substrate, the force increases more rapidly with compression and the distance between oscillations decreases. This is consistent with previous neutron reflectivity data on this

DOI: 10.1021/acs.langmuir.5b01008
Langmuir 2015, 31, 5513−5520

Table 2. Summary of Physical Parameters Measured from C-AFM Force Distance Curves and AM-AFM Imaging

sample ID	L_3, 22 vol %	L_3, 27 vol %	L_3, 32 vol %	L_α, 22 vol %	L_α, 27 vol %	L_α, 32 vol %
oscillation period (nm)	24	15	13	12	11	10
characteristic distance (nm)[15,59]	16	12	10	12	9	8
bulk $\bar{B}$ (kJ/m^3)	8	25	110	100	125	235
AM-AFM passage size (nm)	17.4 ± 1.2	11.4 ± 2.2	9.1 ± 1.0			

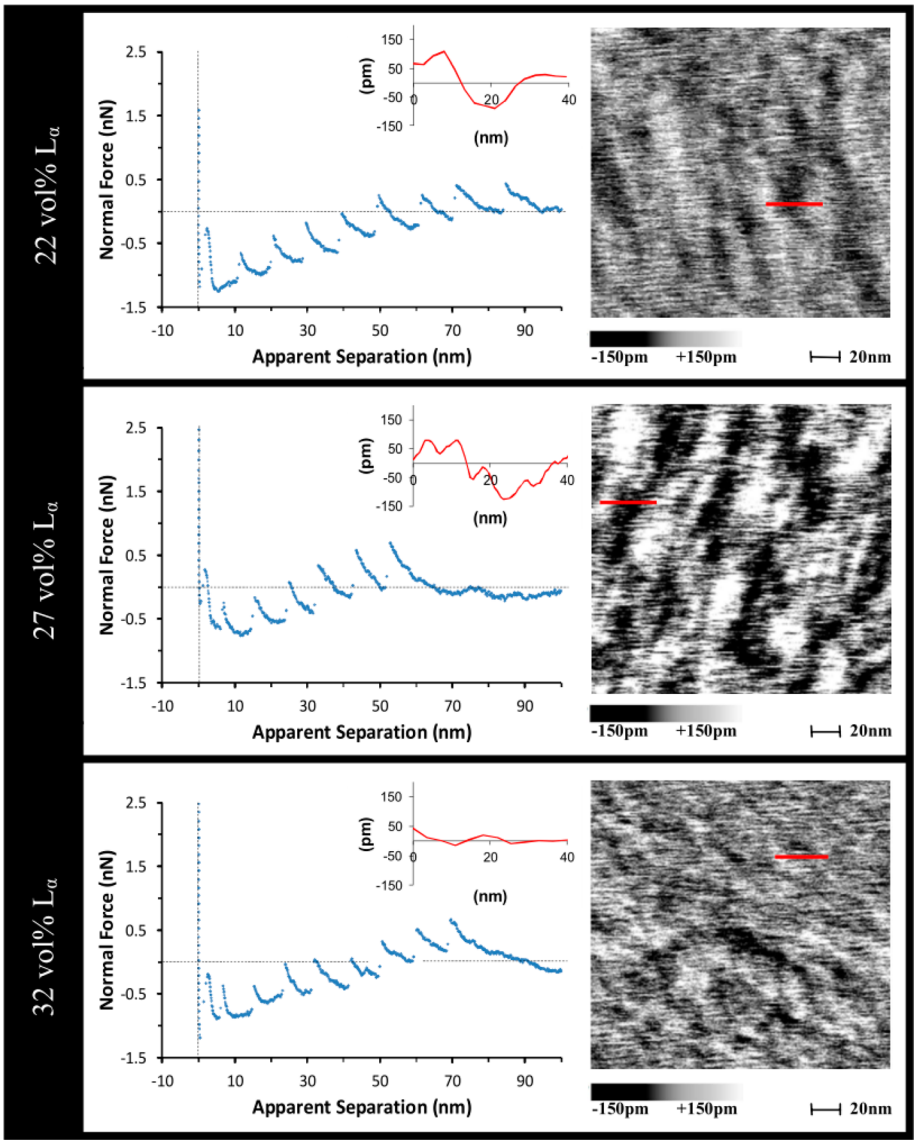

Figure 2. Near surface interfacial data for the L_α system over a range of membrane volume fractions (ϕ = 22, 27, and 32 vol %). Column 1 shows typical force profiles as recorded by the approach of the substrate and AFM tip, with the x axis measuring the displacement of the AFM piezo scanners and the y axis monitoring the force corresponding to deflection of the tip. The inset shows the vertical height variations over a small transect from a cross-sectional cut in column 2. Column 2 shows height images, with dark areas corresponding to areas of depression and related to low-lying areas as a result of undulation.

L_3 phase on quartz,[15] which showed that the substrate breaks the isotropic symmetry of the bulk L_3 phase and a flatter structure results. AM-AFM is used to probe the lateral morphology of the surfactant membrane nearest the surface.

In AM-AFM, imaging of the near surface structure is achieved by oscillating the cantilever at a set working amplitude (A) or "set point" lower than its free amplitude (A_0). The images show that the free amplitude of the cantilever (A_0) was ~1 nm, while A/A_0 was 0.5 ± 0.2. As the sample is scanned line by line, height images are obtained from a feedback loop that constantly readjusts the average tip−sample distance to maintain the working amplitude. To ensure that the tip probed the surfactant membrane nearest the surface, the set point ratio was first decreased until the oscillation amplitude was strongly dampened as a result of the proximity of the surface. The set point was then carefully increased to move the tip away from the substrate into the plane of the first near surface layer. Force profiles in Figure 1 show that the first surface layer is between ~10 and 25 nm thick, depending upon the membrane volume fraction. Because the working oscillation amplitude is much

DOI: 10.1021/acs.langmuir.5b01008
Langmuir 2015, 31, 5513−5520

less, the images can be conceptualized as slices through the near surface structure parallel to the substrate plane. As with any AFM experiment, the absolute tip sample separation is unknown. The images in Figure 1 reveal structures that are much different from worm-like aggregates reported for cationic surfactants adsorbed directly to mica,[56] confirming that it was the near surface structure and not the surface adsorbed film that the AFM tip probed. As the scan size or direction was changed, the image responded accordingly, confirming that features were not artifacts.

Height images of the near surface layer structure for the L_3 phase at membrane volume fractions of 22, 27, and 32 vol % are shown in Figure 1. The appearance of these images is strikingly similar to published schematics of L_3 phases based on Lattice−Boltzmann mathematic models.[57,58] The images consist of dark round areas surrounded by networked lighter areas. The light colors indicate regions where the surface has been moved away from the tip to maintain the oscillation amplitude during imaging. Because the surfactant membrane is less mobile than the solvent,[31] the light, raised areas are associated with the membrane and the dark areas are associated with solvent passages. The fact that these structures can readily be imaged using AM-AFM suggests that the surfactant films have reduced mobility in the vicinity of the surface. As the membrane volume fraction increases, the features in the image decrease in size. Because the thickness of the surfactant bilayer is essentially constant over this concentration range,[31] the decrease in the size of the features is a consequence of the lower solvent content, leading to smaller passages. Therefore, at higher membrane concentrations, the near surface layer membrane structures are spatially constrained within a narrower plane, which makes the sponge structure easier to image and discern visually in the two-dimensional (2D) height image.

The inset to the height image shows a section analysis, which suggests that the average lateral center to center distances between membranes are ∼25, 23, and 9.5 nm for membrane volume fractions of 22, 27, and 32 vol %, respectively. To obtain a representative value for the entire image, a Fourier transform was performed and then radially averaged to produce the 1D plot of intensity as a function of q, the reciprocal space dimension. Both are shown in Figure 1. The low q limit is defined by the image size ($2\pi/150$ nm = 0.03 nm^{-1}), and the upper q limit is set by the width of a scan line. Because there are 256 lines in a single image, the upper q limit is $2\pi/(150/256)$ = 10.7 nm^{-1}; however, the data have been trimmed at 2 nm^{-1} for clarity. For all three membrane concentrations, these plots reveal a single peak that shifts to higher q as the membrane volume fraction increases; the real space distances corresponding to the position of the peak are 28, 20.5, and 12.5 nm for 22, 27, and 32 vol %, respectively. These distances are considerably higher than the oscillation period in the normal force curve for 22 and 27 vol % and approximately equal to the oscillation period for 32 vol %. This shows that, for the lower membrane concentrations, the surface aligns the sponge structure normal to the interface but the lateral structure is less strongly affected. The 32 vol % membrane system is already relatively strongly constrained because of the close proximity of the bilayers (it is closer to a lamellar structure); therefore, the membrane spacing in the surface plane is similar to the oscillation period.

The near surface L_3 phase passage diameters were determined by taking two measurements at 90° to each other for each passage in the image. These values were used to determine the average passage size for each image, shown in Table 2. The bulk phase passage size for each membrane concentration was calculated by fitting a power law to published data.[15] Within error, the average passage size in the near surface layer is the same as the bulk passage size (characteristic distance). Thus, while the surface affects the sponge structure normal to the interface, especially for the lower 22 and 27 vol % membrane volume fractions, the lateral sponge structure is hardly changed.

Normal force curves and height images for the same membrane volume fractions in the L_α phase are presented in Figure 2; the systems are moved into the lamellar region by decreasing the hexanol/CPCl mass ratio to 0.9 hexanol/1 CPCl. The contact mode force curve data consists of a series of oscillations, which for the L_α phase is due to compression of lamellar sheets. For a given membrane volume fraction, the L_α phase oscillation period is reduced in comparison to the L_3 phase, consistent with the change in the structure. Fits to the L_α phase force data have been performed and are presented in Figure B of the Supporting Information. These fits reveal the oscillation period for each concentration, shown in Table 2. For the L_α phase, the oscillation periods are strikingly similar to the bulk phase repeat spacings, consistent with the lamellar stacks arranging at the interface with minimal change to the bulk structure. Like the L_3 phase, the fits fail for the oscillations closest to the substrate; the period is smaller and the force rises more steeply at small separations. Because the lamellar structure can readily pack next to a solid, this suggests that undulations in the membrane are impeded near the surface.[33,60] Because the tip radius is not accurately known, $\overline{B}$ cannot be treated quantitatively. However, the same tip was used for all L_α phase experiments presented; therefore, $\overline{B}$ values can be compared between experiments. Similar to the L_3 phase, $\overline{B}$ increases with the membrane volume fraction because of stronger interactions between sheets (note that different tips were used for the L_3 and L_α phase systems; therefore, $\overline{B}$ values cannot be compared between systems).

An attractive background force is present for the L_α phase oscillations extending ∼70 nm from the surface. Similar attractive forces have been measured previously for L_α phases using the SFA. Richetti et al. suggested that this attraction could be explained in two ways, but the more likely mechanism could not be definitively identified.[54] The first possibility is damping of membrane fluctuations that have amplitudes greater than the space between the approaching mica surfaces. This lowers the entropy of the confined membranes as the separation is decreased, resulting in an osmotic or depletion-like attraction, which favors expulsion of the lamellar phase from confinement. The second possibility is that the order parameter of the structured phase is increased by the proximity of each macroscopic mica surface (which may be enhanced by attractions between the surface and the membranes). In the SFA, the overall free energy decreases with decreasing separation because ordered layers near both surface overlap and reduce the total amount of the more ordered phase, thus producing an attraction. Richetti et al. measured attractive forces for a L_α phase with a membrane volume fraction of ∼25% (composed of sodium dodecyl sulfate and pentanol) at separations up to ∼150 nm, about double that measured here between the surface and the AFM tip for similar volume fractions. The AFM tip is highly curved and, therefore, unlikely to generate the same near surface ordering effect as the macroscopically near planar mica substrate or the two surfaces of the SFA. Thus, it can act as a probe to discriminate between

DOI: 10.1021/acs.langmuir.5b01008
Langmuir 2015, 31, 5513−5520

the two mechanisms. The confining effect of the tip on membrane fluctuations should extend over the same range as the SFA, but its effect on a near surface ordered region on the planar mica substrate only should halve the range of the attractive force, as is observed. This supports the second mechanism, in which individual macroscopic surfaces perturb the mesophase structure rather than being the result of confinement between two surfaces, and is broadly consistent with the changes seen in the sponge structure here and in neutron reflectivity on quartz.[15]

Height images of the L_α phase are shown in Figure 2. The features in these images scaled and rotated as expected with scan size and scan angle. The structures seen in these images are markedly different from those in the L_3 phase at equivalent membrane volume fractions, lacking the lateral periodicity indicative of membrane channels. The vertical range of the L_α phase images is also much smaller than in L_3, as would be expected for undulating stacks. At the highest membrane volume fraction (32 vol %), the image is very smooth, consistent with a lamellar sheet confined between the surface of the solid substrate and the next near surface layer, which is in relatively close proximity because of the low solvent content. As the membrane concentration is reduced to 27 vol %, undulations appear in the near surface lamellar structure. These undulations become clearer and more pronounced when the membrane volume fraction is further reduced to 22 vol %. Reducing the membrane volume increases the interlayer distance, which permits larger undulations. These ideas have previously been proposed,[60] experimentally observed,[33] and are well-accepted, but images of these changes in structure have not previously been obtained.

CONCLUSION

The bulk structures of surfactant L_3 and L_α phases were well-characterized on the basis of radiation scattering measurements and freeze fracture electron microscopy imaging over 20 years ago.[8,23−26] Similarly, forces measured when these phases are compressed between macroscopic solid surfaces have been well-studied using the SFA, with oscillating force profiles measured for both systems. However, while the oscillation period was constant for the L_α phase, changes in the oscillation period for the L_3 phase indicate that it transitions to a lamellar structure when confined.[17,30−32] This difference was attributed to the lamellar structure being easily accommodated, as opposed to the sponge structure, where the three-dimensional (3D) bulk symmetry is necessarily broken by the surfaces. The structure of these phases near isolated solid surfaces is more difficult to probe and, consequently, less well studied. Neutron reflectivity measurements and model fitting for the CPCl−hexanol−brine system revealed that the bulk L_3 phase persisted near a quartz surface at low concentrations. At higher concentrations, the L_3 to L_α phase transition was noted, but at intermediate concentrations, morphologies transitional to the L_3 and L_α phases were suggested. In this work, we have shown that the high sensitivity of AM-AFM enables delicate near surface surfactant structures to be probed and used AM-AFM to resolve the structures at intermediate membrane concentrations for the CPCl−hexanol−0.2 M NaCl system.

AM-AFM images of the L_3 phase reveal solvent-filled passages surrounded by a networked surfactant membrane. When the membrane volume fraction is increased, the size of the passages decreases because of the greater interfacial area. Analyzing AM-AFM images and contact mode force curves in combination reveals that, at low membrane concentrations, the substrate aligns the sponge structure strongly normal to the interface but relatively weakly laterally. When the membrane concentration is increased, the system is already relatively strongly constrained because of the close proximity of the bilayers (it is closer to a lamellar structure) and the lateral structure is more strongly affected.

The AM-AFM images of the L_α phase suggest that much flatter structures are present than for the L_3 phase, consistent with lamellar sheets aligned in the plane of the surface. At the highest membrane concentration probed, the image is smooth because the sheet is confined between the surface and the next near surface layer, which is in close proximity because of the low solvent content. Lowering the membrane concentration increases the separation between near surface layers, allowing undulations to appear in the near surface lamellar structure. These undulations become more pronounced as the membrane volume fraction is further reduced.

Contact mode AFM force curves for the L_α phase show an attractive background superimposed on the oscillating force data extending approximately 70 nm away from the surface. Similar attractive forces have been measured previously for L_α phases using the SFA, but they extended about 150 nm from the surface. The reduction in the range of the attraction is attributed to the curvature of the AFM tip, meaning that it is unable to generate the strong near surface ordering like a macroscopically near planar mica substrate. This suggests that the origin of the attractive force is an increase in the order parameter of the structured phase caused by the proximity of the mica surface.[33,54]

ASSOCIATED CONTENT

Supporting Information

L_3 (Figure A) and L_α (Figure B) phase normal force data fitted with parabolic overlays, with the oscillation period determined from the distance between adjacent minima, and nominal tip radius (nm) for cantilevers used (Table A). The Supporting Information is available free of charge on the ACS Publications website at DOI: 10.1021/acs.langmuir.5b01008.

AUTHOR INFORMATION

Corresponding Author

*E-mail: rob.atkin@newcastle.edu.au.

Notes

The authors declare no competing financial interest.

REFERENCES

(1) Schramm, L. L.; Stasiuk, E. N.; Marangoni, D. G. Surfactants and their application. *Annu. Rep. Prog. Chem., Sect. C: Phys. Chem.* **2003**, 3−48.

(2) Tiddy, G. J. T. Surfactant-water liquid crystal phases. *Phys. Rep.* **1980**, *57*, 1−46.

(3) Mitchell, D. J.; Tiddy, G. J. T.; Waring, L.; Bostock, T.; McDonald, M. P. Phase behaviour of polyoxyethylene surfactants with water. Mesophase structures and partial miscibility (cloud points). *J. Chem. Soc., Faraday Trans. 1* **1983**, *79*, 975.

(4) Evans, D. F.; Kaler, E. W.; Benton, W. J. Liquid crystals in a fused salt: *β,γ*-Distearoylphosphatidylcholine in *N*-ethylammonium nitrate. *J. Phys. Chem.* **1983**, *87*, 533−535.

(5) Funari, S. S.; Holmes, M. C.; Tiddy, G. J. T. Microscopy, X-ray diffraction, and NMR studies of lyotropic liquid crystal phases in the $C_{22}EO_8$/water system. A new intermediate phase. *J. Phys. Chem.* **1992**, *96*, 11029−11038.

DOI: 10.1021/acs.langmuir.5b01008
Langmuir 2015, 31, 5513−5520

(6) Henriksson, U.; Blackmore, E. S.; Tiddy, G. J. T.; Soderman, O. Intermediate liquid crystalline phases in the binary system $C_{16}TACl-H_2O$: An NMR and low-angle X-ray diffraction study. *J. Phys. Chem.* **1992**, *96*, 3894−3902.
(7) Porte, G.; Marignan, J.; Bassereau, P.; May, R. Shape transformations of the aggregates in dilute surfactant solutions—A small-angle neutron scattering study. *J. Phys.* **1988**, *49*, 511−519.
(8) Strey, R., et al. Fluid Membranes in the Water NaCl-AOT System − A Study Combining Small-Angle Neutron Scattering, Electron-Microscopy and NMR Self-Diffusion. In *Structure and dynamics of strongly interacting colloids and supramolecular aggregates in solution*. Kluwer Academic Publishers: Dordrecht, Netherlands, 1992.
(9) Gazeau, D., et al. Experimental-Evidence for Bicontinuous Structures in L_3 Phases. In *Trends in Colloid and Interface Science III*; Bothorel, P., Dufourc, E. J., Eds.; Dr. Dietrich Steinkopff: Verlag, Berlin, 1989; pp 226−232.
(10) Cates, M. E.; Roux, D.; Andelman, D.; Milner, S. T.; Safran, S. A. Random surface model of the L_3 phase of dilute surfactant solutions. *Europhys. Lett.* **1988**, *5*, 733−739.
(11) Strey, R.; Schomacker, R.; Roux, D.; Nallet, F.; Olsson, U. Dilute lamellar and L_3 phases in the binary water−$C_{12}E_5$ system. *J. Chem. Soc., Faraday Trans.* **1990**, *86*, 2253−2261.
(12) Holmberg, K.; Jonsson, B.; Kronberg, B.; Lindman, B. *Surfactants and Polymers in Aqueous Solution*; John Wiley and Sons: Chichester, U.K., 2002.
(13) Zapf, A.; Hornfeck, U.; Platz, G.; Hoffmann, H. Investigation of the L_3 phase in systems containing calcium dodecyl culfate, alcohol, and water. *Langmuir* **2001**, 6113−6118.
(14) Fontell, K. Influence of electrolyte on phase equilibria and phase structure in the binary system of di-2-ethylhexyl sulphosuccinate and water. In *Colloidal Dispersions and Micellar Behavior*; Mittal, K. L., Ed.; American Chemical Society (ACS): Washington, D.C., 1975; ACS Symposium Series, Vol. *9*; Chapter 19, pp 270−277.
(15) Hamilton, W. A.; Butler, P. D.; Warr, G. G. Local membrane ordering of sponge phases at a solid−solution interface. *J. Chem. Phys.* **2002**, *116*, 8533−8546.
(16) Nastishin, Y.; Lambert, E.; Boltenhagen, P. Temperature-induced structural transitions of the quasi-ternary system cetylpyridinium chloride−hexanol−brine. *C. R. Acad. Sci., Ser. IIb: Mec., Phys., Chim., Astron.* **1995**, *321*, 205−210.
(17) Antelmi, D. A.; Kékicheff, P.; Richetti, P. Measurement of the interactions between macroscopic surfaces inducing a 1st-order phase-transitions—The sponge lamellar transformation. *J. Phys. II* **1995**, *5*, 103−112.
(18) Yamamoto, J.; Tanaka, H. Shear-induced sponge-to-lamellar transition in a hyperswollen lyotropic system. *Phys. Rev. Lett.* **1996**, *77*, 4390−4393.
(19) Porcar, L.; Hamilton, W. A.; Butler, P. D.; Warr, G. G. Scaling of shear-induced transformations in membrane phases. *Phys. Rev. Lett.* **2002**, *89*, 168301.
(20) Porcar, L.; Hamilton, W. A.; Butler, P. D.; Warr, G. G. Topological relaxation of a shear-induced lamellar phase to sponge equilibrium and the energetics of membrane fusion. *Phys. Rev. Lett.* **2004**, *93*, 198301.
(21) Butler, P. D.; Porcar, L.; Hamilton, W. A.; Warr, G. G. A Vapor Barrier Couette Shear Cell For Small Angle Neutron Scattering Measurements. *Rev. Sci. Instrum.* **2002**, *73* (6), 2345−2354.
(22) Porte, G.; Appell, J.; Bassereau, P.; Marignan, J. L_α to L_3—A topology driven transition in phases of infinite fluid membranes. *J. Phys.* **1989**, *50*, 1335−1347.
(23) Maldonado, A.; Urbach, W.; Ober, R.; Langevin, D. Swelling behavior and local topology of an L_3 (sponge) phase. *Phys. Rev. E: Stat. Phys., Plasmas, Fluids, Relat. Interdiscip. Top.* **1996**, *54*, 1774−1778.
(24) Skouri, M.; Marignan, J.; May, R. X-ray and neutron-scattering study of the lamellar and L_3 phases of the system aerosol-ot-water—Effect of nacl and decane. *Colloid Polym. Sci.* **1991**, *269*, 929−937.
(25) Strey, R.; Jahn, W.; Porte, G.; Bassereau, P. Freeze fracture electron microscopy of dilute lamellar and anomalous isotropic (L_3) phases. *Langmuir* **1990**, *6*, 1635−1639.
(26) Hoffmann, H.; Thunig, C.; Munkert, U.; Meyer, H. W.; Richter, W. From vesicles to the L_3 (sponge) phase in alkyldimethylamine oxide heptanol systems. *Langmuir* **1992**, *8*, 2629−2638.
(27) Porcar, L.; Hamilton, W. A.; Butler, P. D.; Warr, G. G. Scaling of structural and rheological response of L_3 sponge phases in the "sweetened" cetylpyridinium/hexanol/dextrose/brine system. *Langmuir* **2003**, *19*, 10779−10794.
(28) Nastishin, Y. A.; Dovgyi, O. B.; Kostruba, A. M. The study of the interface between the L_3 (sponge) phase and a solid substrate. In *Nonlinear Optics of Liquid and Photorefractive Crystals II*; Klimusheva, G. V., Ed.; Proceedings of the Society of Photo-Optical Instrumentation Engineers (SPIE); SPIE—International Society for Optical Engineering: Bellingham, WA, 1998; Vol. *3488*, pp 156−163.
(29) Nastishin, Y. A.; Dovgyi, O. B.; Kostruba, A. M. Optical study of the interface between the lyotropic L_3 (sponge) phase and solid substrate. *Ukr. J. Phys. Opt.* **2000**, *1*, 96−102.
(30) Petrov, P.; Olsson, U.; Christenson, H.; Miklavic, S.; Wennerstroem, H. Forces between macroscopic surfaces in a sponge phase. *Langmuir* **1994**, *10*, 988−990.
(31) Petrov, P.; Miklavcic, S.; Olsson, U.; Wennerstrom, H. A confined complex liquid—Oscillatory forces and lamellae formation from an L_3 phase. *Langmuir* **1995**, *11*, 3928−3936.
(32) Antelmi, D. A.; Kékicheff, P.; Richetti, P. The confinement-induced sponge to lamellar phase transition. *Langmuir* **1999**, *15*, 7774−7788.
(33) Kekicheff, P.; Christenson, H. K. Forces measured in a swollen lyotropic lamellar mesophase confined between solid surfaces. *Phys. Rev. Lett.* **1989**, *63*, 2823−2826.
(34) Segura, J. J.; Elbourne, A.; Wanless, E. J.; Warr, G. G.; Voitchovsky, K.; Atkin, R. Adsorbed and near surface structure of ionic liquids at a solid interface. *Phys. Chem. Chem. Phys.* **2013**, *15*, 3320−3328.
(35) Page, A. J.; Elbourne, A.; Stefanovic, R.; Addicoat, M. A.; Warr, G. G.; Voitchovsky, K.; Atkin, R. 3-Dimensional atomic scale structure of the ionic liquid−graphite interface elucidated by AM-AFM and quantum chemical simulations. *Nanoscale* **2014**, *6*, 8100−8106.
(36) Elbourne, A.; Sweeney, J.; Webber, G. B.; Wanless, E. J.; Warr, G. G.; Rutland, M. W.; Atkin, R. Adsorbed and near-surface structure of ionic liquids determines nanoscale friction. *Chem. Commun.* **2013**, *49*, 6797−6799.
(37) Ueno, K.; Kasuya, M.; Watanabe, M.; Mizukami, M.; Kurihara, K. Resonance shear measurement of nanoconfined ionic liquids. *Phys. Chem. Chem. Phys.* **2010**, *12*, 4066−4071.
(38) Elbourne, A.; Voitchovsky, K.; Warr, G. G.; Atkin, R. Ion structure controls ionic liquid near-surface and interfacial nanostructure. *Chem. Sci.* **2015**, *6*, 527−536.
(39) Smith, A. M.; Lovelock, K. R. J.; Gosvami, N. N.; Licence, P.; Dolan, A.; Welton, T.; Perkin, S. Monolayer to bilayer structural transition in confined pyrrolidinium-based ionic liquids. *J. Phys. Chem. Lett.* **2013**, *4*, 378−382.
(40) Li, H.; Endres, F.; Atkin, R. Effect of alkyl chain length and anion species on the interfacial nanostructure of ionic liquids at the Au(111)−ionic liquid interface as a function of potential. *Phys. Chem. Chem. Phys.* **2013**, *15*, 14624−14633.
(41) Werzer, O.; Cranston, E. D.; Warr, G. G.; Atkin, R.; Rutland, M. W. Ionic liquid nanotribology: Mica−silica interactions in ethylammonium nitrate. *Phys. Chem. Chem. Phys.* **2012**, *14*, 5147−5152.
(42) Li, H.; Rutland, M. W.; Atkin, R. Ionic liquid lubrication: Influence of ion structure, surface potential and sliding velocity. *Phys. Chem. Chem. Phys.* **2013**, *15*, 14616−14623.
(43) Li, H.; Wood, R. J.; Rutland, M. W.; Atkin, R. An ionic liquid lubricant enables superlubricity to be "switched on" in situ using an electrical potential. *Chem. Commun.* **2014**, *50*, 4368−4370.
(44) Sweeney, J.; Webber, G. B.; Rutland, M. W.; Atkin, R. Effect of ion structure on nanoscale friction in protic ionic liquids. *Phys. Chem. Chem. Phys.* **2014**, *16*, 16651−16658.
(45) Li, H.; Cooper, P. K.; Somers, A. E.; Rutland, M. W.; Howlett, P. C.; Forsyth, M.; Atkin, R. Ionic liquid adsorption and nanotribology at the silica−oil interface: Hundred-fold dilution in oil lubricates as

DOI: 10.1021/acs.langmuir.5b01008
Langmuir 2015, 31, 5513−5520

effectively as the pure ionic liquid. *J. Phys. Chem. Lett.* **2014**, *5*, 4095−4099.
(46) Mezger, M.; Schroder, H.; Reichert, H.; Schramm, S.; Okasinski, J. S.; Schoder, S.; Honkimaki, V.; Deutsch, M.; Ocko, B. M.; Ralston, J.; Rohwerder, M.; Stratmann, M.; Dosch, H. Molecular layering of fluorinated ionic liquids at a charged sapphire (0001) surface. *Science* **2008**, *322*, 424−428.
(47) Perkin, S.; Albrecht, T.; Klein, J. Layering and shear properties of an ionic liquid, 1-ethyl-3-methylimidazolium ethylsulfate, confined to nano-films between mica surfaces. *Phys. Chem. Chem. Phys.* **2010**, *12*, 1243−1247.
(48) Perkin, S.; Crowhurst, L.; Niedermeyer, H.; Welton, T.; Smith, A. M.; Gosvami, N. N. Self-assembly in the electrical double layer of ionic liquids. *Chem. Commun.* **2011**, *47*, 6572−6574.
(49) Hayes, R.; Borisenko, N.; Corr, B.; Webber, G. B.; Endres, F.; Atkin, R. Effect of dissolved LiCl on the ionic liquid−Au(111) electrical double layer structure. *Chem. Commun.* **2012**, *48*, 10246−10248.
(50) Hyde, S. T. Identification of lyotropic liquid crystalline mesophases. *Handb. Appl. Surf. Colloid Chem.* **2001**, 299−332.
(51) Haugstad, G. *Atomic Force Microscopy*; John Wiley & Sons, Inc.: Hoboken, NJ, 2012; p 520.
(52) Hutter, J. L.; Bechhoefer, J. Calibration of atomic force microscope tips. *Rev. Sci. Instrum.* **1993**, *64*, 1868−1873.
(53) Eastman, T.; Zhu, D. M. Adhesion forces between surface-modified AFM tips and a mica surface. *Langmuir* **1996**, *12*, 2859−2862.
(54) Richetti, P.; Kekicheff, P.; Barois, P. Measurement of the layer compressibility modulus of a lamellar mesophase with a surface forces apparatus. *J. Phys. II* **1995**, *5*, 1129−1154.
(55) Richetti, P.; Kekicheff, P.; Parker, J. L.; Ninham, B. W. Measurement of the interactions between membranes in a stack. *Nature* **1990**, *346*, 252−254.
(56) Ducker, W. A.; Wanless, E. J. Adsorption of hexadecyltrimethylammonium bromide to mica: Nanometer-scale study of binding-site competition effects. *Langmuir* **1999**, *15*, 160−168.
(57) Gonzalez-Segredo, N.; Coveney, P. V. Self-assembly of the gyroid cubic mesophase: Lattice−Boltzmann simulations. *Europhys. Lett.* **2004**, *65*, 795−801.
(58) Gonzalez-Segredo, N.; Coveney, P. V. Coarsening dynamics of ternary amphiphilic fluids and the self-assembly of the gyroid and sponge mesophases: Lattice−Boltzmann simulations. *Phys. Rev. E: Stat., Nonlinear, Soft Matter Phys.* **2004**, *69*, 1−30.
(59) Quilliet, C.; Blanc, C.; Kleman, M. Evidence of a phenomenon of epitaxy at the interface between a lamellar L_α phase and a L_3 sponge. *Phys. Rev. Lett.* **1995**, *77*, 522−525.
(60) Janke, W.; Kleinert, H.; Meinhart, M. Monte-Carlo study of a stack of self-avoiding surfaces with extrinsic curvature stiffness. *Phys. Lett. B* **1989**, *217*, 525−529.

DOI: 10.1021/acs.langmuir.5b01008
Langmuir 2015, 31, 5513−5520